# Ideal compressive strength of fcc Co, Ni, and Ni-rich alloys along the ⟨001⟩ direction: A first-principles study

A. Breidi,[1,*] S. G. Fries,[1] and A. V. Ruban[2,3]

[1]*The Interdisciplinary Centre for Advanced Materials Simulation (ICAMS), Ruhr Universität Bochum, Universität Straße 150, 44801 Bochum, Germany*

[2]*Department of Materials Science and Engineering, Kungliga Tekniska högskolan (KTH), SE-100 44 Stockholm, Sweden*

[3]*Materials Center Leoben Forschung GmbH, A-8700 Leoben, Austria*

(Received 7 October 2015; revised manuscript received 11 February 2016; published 7 April 2016)

We perform density functional theory based first-principles calculations to identify promising alloying elements ($X$) capable of enhancing the compressive uniaxial theoretical (ideal) strength of the fcc Ni-matrix along the ⟨001⟩ direction. The alloying element belongs to a wide range of 3$d$, 4$d$, and 5$d$ series with nominal composition of 6.25 at. %. Additionally, a full elastic study is carried to investigate the ideal strength of fcc Ni and fcc Co. Our results indicate that the most desirable alloying elements are those with half $d$-band filling, namely, Os, Ir, Re, and Ru.

DOI: 10.1103/PhysRevB.93.144106

## I. INTRODUCTION

The mechanical strength and structural stability of a crystal under axial loading or shearing are primary issues for engineering materials. In real materials, the strength is determined by the complex microstructural properties associated with defects, such as vacancies, dislocation networks, and grain boundaries. A mechanical failure occurs when applied stresses exceed mechanical strength of the imperfect-weakest region of the lattice. The *effective theoretical (ideal) strength* [1] (ETS) of a crystal is indicated by the stress and strain values at which the crystal becomes mechanically unstable in terms of Born criteria, while the *maximum theoretical strength* [2] (MTS) corresponds to the first maximum/minimum of the stress-strain curve. A realistic description of strength involving precise modeling of the dislocation activity for long periods of time poses a great challenge and renders standard electronic structure calculations unfeasible. However, the theoretical strength of solids has an upper bound or limit which is referred to as the ideal theoretical strength [2] (ITS). The ideal strength has been considered as a primary intrinsic mechanical parameter of single crystal materials [3–5], because it relates features of chemical bonding and crystal chemistry with the mechanical properties of perfect lattices, such as bond switching or breaking, common slip [3], initiation of failure or nucleation of cracks or dislocations [2,6], as demonstrated by nanoindentation experiments [7], and thus should be an essential mechanical parameter of materials.

Perfect crystals, throughout homogeneous by definition, would fail as a result of the lattice as a whole becomes mechanically unstable. In this sense, "fail" means the upper limit of the theoretical strength of a real crystalline material. This instability occurs when the lattice, in the presence of the applied forces, can lower its total energy by spontaneously undergoing an additional arbitrary set of small uniform deformations. However, other instabilities may occur under homogeneous deformation of a solid, e.g., related to phonons [3,8–12].

Nickel is chiefly valuable in the modern world for the alloys it forms, thanks to its excellent mechanical properties such as hardness and ductility, and its high melting point. About 60% of world production comes into nickel steels and the remainder is used in new Ni-base superalloys. On the other hand, cobalt is characterized by a higher melting point, where cobalt-base superalloys are the second-largest share of the total end use of its productions. The temperature stability of Co-base alloys makes them suitable for use in turbine blades for gas turbines and jet aircraft engines, though nickel-base single crystal alloys surpass them in this regard [13].

Important efforts have been made to understand the behavior of elemental solids [14–16], compounds [17–23] at the atomic level. Studies, so far, have focused on elemental nickel, and no theoretical effort, to the best of our knowledge, has been made to investigate solid solution strengthening of nickel, which can be understood due to the tremendous amount of time and calculations needed to treat properly low symmetry systems, i.e., random alloys.

The ideal strength of Ni under uniaxial loading in a ⟨001⟩ direction has been studied long time ago by Milstein [24] using semiempirical approaches when describing interatomic interactions. However, within such schemes, parameters are fitted predominantly to equilibrium properties of the material studied, so that their transferability to the loaded states are not guaranteed. In contrast, first-principles electronic structure calculations based on density functional theory can be performed reliably for variously strained structures and are thus capable of determining the theoretical strength without resort to untrustful extrapolations. Recently, Černý and Pokluda [25,26] calculated the maximum theoretical strength $\sigma_{\max}$ and the ultimate strain $\epsilon_{\max}$ of Ni under uniaxial tension and compression for ⟨001⟩, ⟨110⟩, and ⟨111⟩ orientations of the loading axis. Liu *et al.* [27] investigated the maximum theoretical shear strength in the slip systems {111}⟨112⟩ and {111}⟨110⟩. Consequently, it turns out that the compressive stress along the direction ⟨001⟩ (7.1 GPa) [24] and the shear stress in the slip systems {111}⟨112⟩ (5.1 GPa) [27] are the weakest. It follows that the different loading modes [24–27] produced different theoretical strengths, however, the lowest one is the most pertinent for the onset of dislocations motion. In this regard, the corresponding mode is the weakest link when analyzing a complex distorted environment dislocation cores, grain boundaries, and other

*Present address: School of Metallurgy and Materials - University of Birmingham; a.breidi@hotmail.com

 

| 3 | 4 | 5 | 6 | 7 | 8 | 9 | 10 | 11 | 12 |
|---|---|---|---|---|---|---|---|---|---|
| Sc | Ti | V | Cr | Mn | Fe | Co | Ni | Cu | Zn |
| Y | Zr | Nb | Mo | Tc | Ru | Rh | Pd | Ag | Cd |
| La | Hf | Ta | W | Re | Os | Ir | Pt | Au | Hg |

FIG. 1. Atoms (within the gray background) used in this study as alloying elements added to the nickel matrix to form Ni-6.25 at. % $X$ random alloys.

extended defect with decisive impact on materials plasticity and strength.

In the light of this background, the core issue we investigate is strengthening the Ni matrix with transition metal (TM) alloying elements at a particular alloy composition, 6.25 at. % specifically. The loading mode is the uniaxial compressive direction ⟨001⟩ because it is the weakest uniaxial load. We seek answers to several core questions: Which alloying atoms induce strengthening or embrittlement effects? How significant could such effects be? Does fcc Co possess higher or lower ideal strength than fcc Ni? How do Ni and Co fail in compressive uniaxial stress?

In the present paper we employ first principles supercell method to investigate in depth the abovementioned issues. The studied systems are elemental Ni and Co, and the $Ni_{1-x}X_x$ alloys (limiting to $x = 6.25$ at. %, or $x = 1/16$), with most of $3d$ (Ti through Zn), $4d$ (Zr through Cd), and $5d$ (Hf through Au) alloying element species $X$ (see Fig. 1). The composition 6.25 was specifically chosen because it allows us to generate reasonably big supercells having optimized correlation functions, very close to the real chemically disordered alloys at this very composition. Moreover, this composition is of practical interest because it represents an average value of the various refractory TM elements added to the Ni matrix to form Ni-base superalloys.

We predict that the ideal strength of Ni can be significantly altered *via* alloying. We demonstrate that strengthening effect *via* solid solution is heavily related to the alloying element $d$-electron number. We give evidence to support this argument by comparing with available experimental data and previous investigations done on elemental TM solids.

## II. COMPUTATIONAL METHOD

### A. Theory: uniaxial load

For the case of *unconstrained* uniaxial load on fcc crystal, an external stress is applied perpendicular to a cube face, say along the ⟨001⟩ direction, parallel to the $a_1$ axis. All of the three angles will retain their initial values of $\frac{\pi}{2}$ until the crystal fails. As the edge $a_1$ incrementally contracts, the edges $a_2$ and $a_3$, by symmetry, will elongate, where $a_2 = a_3$ is seen to be maintained by symmetry.

The equilibrium state $(a_1^k, a_2^k, a_3^k)$ is determined through minimizing the total energy by relaxing the stresses $\sigma_2^k$ and $\sigma_3^k$ in the direction perpendicular to the loading axis

$$\left(\frac{\partial E}{\partial a_2}\right)_{(a_1^k, a_2^k, a_3^k)} = 0, \tag{1a}$$

$$\left(\frac{\partial E}{\partial a_3}\right)_{(a_1^k, a_2^k, a_3^k)} = 0. \tag{1b}$$

The above equations satisfy the unconstrained nature of the applied stress, implying

$$\sigma_2^k = \sigma_3^k = 0\,, \tag{2a}$$

$$\sigma_1^k = \frac{1}{a_1^0 \times a_2^k \times a_3^k}\left(\frac{\partial E}{\partial \epsilon_1^k}\right)_{(a_1^k, a_2^k, a_3^k)}, \tag{2b}$$

where $E$ is the total energy per (super) cell, $\epsilon_1^k = \frac{(a_1^k - a_1^0)}{a_1^0}$ is the uniaxial strain, $a_1^0$ is the lattice parameter of the original unstrained fcc lattice, and $a_2^k \times a_3^k$ is the area of the basis of the cell in the plane perpendicular to the loading axis. The inflexion point in the $(E - \epsilon_1^k)$ curve, or the first minimum point of the $(\sigma_1^k - \epsilon_1^k)$ curve provides the maximum (in absolute value) theoretical compressive strength (MTCS). MTCS is given by Eqs. (2) which correspond to conditions for the strained lattice to be in equilibrium with respect to internal and external forces. However, the tetragonal lattice may become in unstable equilibrium prior to reaching the inflexion point, in the possible case of hitting an instability point, such as soft phonon modes, violation of Born criteria for stability, or magnetic spin arrangement. In principle, the analysis of the phonon spectrum of a strained lattice at each equilibrium state along the loaded path is necessary and sufficient to ascertain the stability of the investigated material; but such calculations based on DFT are extremely time demanding and were performed only for tensile tests in pure Al [8–12,15]. In our study, we probe the mechanical stability of cubic crystals in terms of Born criteria under uniaxial load as derived by Hill *et al.* [28] and Milstein [1], which emphasize that there must be a positive expenditure of energy on going from the *stable* equilibrium state $(a_1^k, a_2^k, a_3^k)$ to any nearby state *via* small homogeneous deformations. Thereby, the conditions imposed on the elastic stiffness constants are [1]

$$C_{11} > 0\,; \tag{3a}$$

$$C_{55} > 0\,; \tag{3b}$$

$$C_{44} > 0\,; \tag{3c}$$

$$C_{22} - C_{23} > 0\,; \tag{3d}$$

$$(C_{22} + C_{23}) - \frac{2C_{12}^2}{C_{11}} > 0\,, \tag{3e}$$

where

$$C_{ij} = \frac{1}{a_1^k \times a_2^k \times a_3^k}\left(\frac{\partial^2 E}{\partial \epsilon_i \partial \epsilon_j}\right)_{(a_1^k, a_2^k, a_3^k)}, \tag{4}$$

and the strains in this case are expressed as

$$\epsilon_i = \frac{a_i - a_i^k}{a_i^k} \quad i = 1,2,3\,; \tag{5a}$$

$$\epsilon_i = a_i - a_i^k \quad i = 4,5,6\,, \tag{5b}$$

where $a_4$, $a_5$, and $a_6$ are the angles between the tetragonal cell edges $a_2$ and $a_3$, $a_1$ and $a_3$, and $a_1$ and $a_2$, respectively.

The above relations are the necessary and sufficient conditions for the lattice to be in *stable equilibrium* in terms of Born criteria. In applying the above formalism, one proceeds through determining the equilibrium state $(a_1^k, a_2^k, a_3^k)$ at every

strain $\epsilon_k^1$ through employing Eqs. (1). Subsequently, one must calculate the whole set of tetragonal elastic constants in order to determine if the lattice would be stable in this state, as illustrated in Eqs. (3). This process is continued until one of the stability relations is violated. The value of $\sigma_1^k$ at which the instability occurs is the effective theoretical compressive strength (ETCS) of the crystal and $\frac{(a_1^k - a_1^0)}{a_1^0}$ is the effective theoretical compressive strain.

### B. First-principles calculations

In this paper we investigate random alloys neglecting the contribution from possible short-range order effects. These alloys are modeled by a 128-atom fcc-based $4 \times 4 \times 2(\times 4)$ supercell. To get random distribution of atoms we minimize the Warren-Cowley short-range order (SRO) parameters [29,30] at several nearest neighbor coordination shells. We found the SRO parameters to be less than 0.002 at the first eight coordination shells. The projector augmented wave (PAW) method [31] implemented in the Vienna first-principles simulation package (VASP) [32–34] was used to calculate total energies. The exchange correlation energy was treated in the GGA with the PBE96 functional [35]. After necessary tests to control the stability of energy, the energy cutoff was set to 350 eV. In accordance with the supercell size, in the self-consistent calculations, we have used $4 \times 4 \times 8$ Monkhorst-Pack $k$-point mesh [36].

All the calculations are done either neglecting spin polarization considering that the state is nonmagnetic (NM), or in the ferromagnetic (FM) state. The operational temperature of Ni, Co, and Ni-rich alloys, within the domain of their applications, is beyond 1200 K. Consequently, in the proximity of this temperature fcc Ni and Ni-rich alloys are paramagnetic, while fcc Co is ferromagnetic. In the considered Ni-6.25 at. % $X$ alloys, at low temperatures, spin-polarization effects become very weak. However, it is not most probably true for the high temperature states, where local magnetic moment on Ni can survive due to longitudinal spin fluctuations [37]. Nevertheless, we neglect these effects, as we do not include thermal excitations in the present investigation.

## III. fcc Ni and Co

It is important to mention here that the ground state structure of Cobalt is hcp [38]. However, it undergoes a phase transition to fcc at $690 \pm 6$ K [38]. The fcc phase is ferromagnetic (FM) below the curie temperature (1388 K) [39]. In fact, our interest in studying the uniaxial ideal strength of the fcc FM phase of Co is motivated by its intermediate and high temperature applications. In accordance with the methodology described in Sec. II, we conducted simulations of the compressive test in pure fcc Ni and fcc Co. The corresponding strain energies as a function of the compressed axial parameter $a_1$ are displayed in Fig. 2(a). As manifested in Fig. 2(a) the strain-energy profiles have a parabolic, symmetry-dictated convex character centered around the fcc ground state. Upon decreasing $a_1$, the strain reach their inflexion points (marked by blue vertical lines) due to non-linear effects, which correspond to the MTCS.

The compressive stresses calculated according to Eq. (2b) are shown in Fig. 4. The inflexion points at the energy vs strain

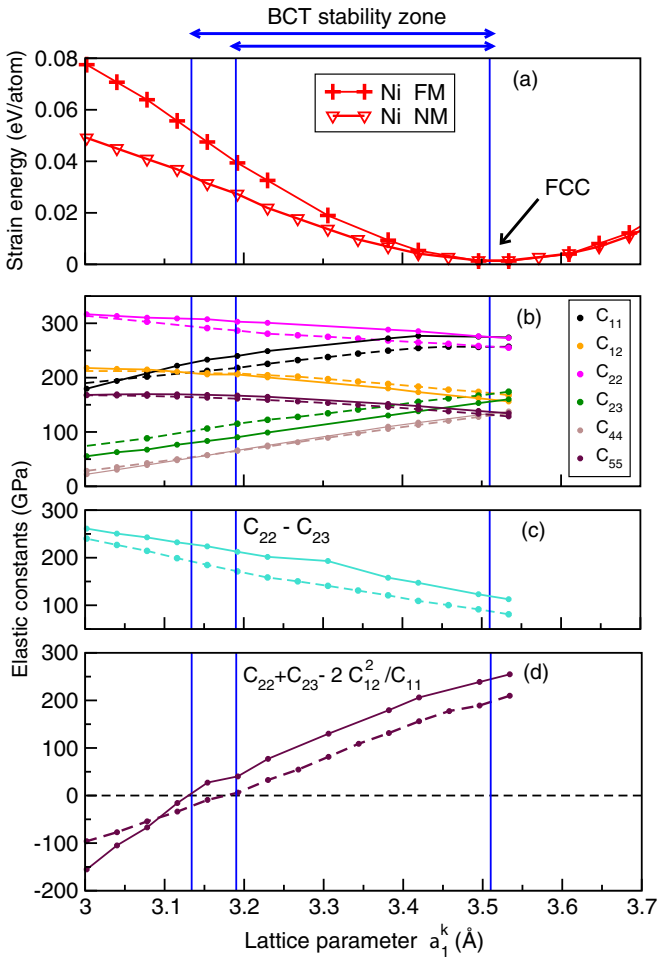


FIG. 2. (a) Strain energy of fcc Ni (b) variation in the elastic constants related to face-centered tetragonal lattice as given by Eqs. (4), (c) Born criteria of stability Eq. (3d), and (d) Eq. (3e) of NM (dashed-lines) and FM (solid-lines) Ni, along the tetragonal deformation path as a function of the compressed [001] axial parameter $a_1^k$. The blue vertical lines mark the values of the lattice parameters $a_1^k$ at which the lattice is stress-free (right line) or becomes unstable (left lines).

curves (represented by the lattice constant $a_1^k$ in Figs. 2 and 3), respectively, correspond to maximum stresses NM/FM Ni and FM Co can sustain if their structures type do not undergo a phase transition prior to the relevant elastic limits (inflexion points). A comparison of MTCS values obtained by us and by others are shown in Table I. We reproduce almost exactly the MTCS value (9.37 GPa) of FM Ni obtained earlier [26] (9.40 GPa). For NM Ni our MTCS (5.93 GPa) differs from that reported in Ref. [24] (7.1 GPa). We attribute this difference to less accurate description of interatomic interaction in the latter paper. On the other hand, we determined the MTCS value for fcc FM Co to be 8.20 GPa. Unfortunately, we can't compare it with results obtained by other methods because, to best of our knowledge, no previous works have treated the theoretical strength of fcc Co. In fact, it makes sense to compare MTCS of FM Co and NM Ni and not FM Ni, because of their high-temperature applications where Ni is paramagnetic and Co is ferromagnetic. In this regard, we note that FM Co MTCS value (8.20 GPa) is larger than NM Ni (5.93 GPa) by 27.6%.

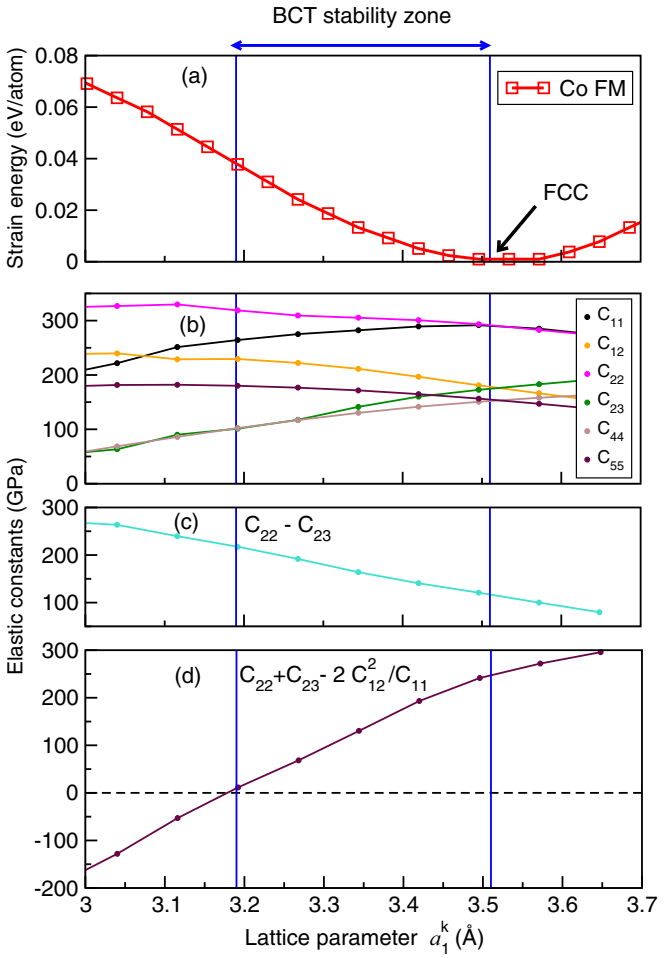


FIG. 3. (a) Strain energy of fcc FM Co (b) variation in the elastic constants related to face-centered tetragonal lattice, (c) Born criteria of stability Eq. (3d), and (d) Eq. (3e), along the tetragonal deformation path as a function of the compressed [001] axial parameter $a_1^k$.

To be certain that the MTCS values are indeed the ETCS ones and to determine the mode of failure of fcc Ni and Co crystals, we examine their mechanical stabilities at every applied load according to Born criteria. We should mention here that this type of study is essential to check if an instability comes forth before the inflexion point has been reached. Hence, we calculated the six independent face-centered tetragonal elastic constants as functions of lattice parameter $a_1^k$ using Eqs. (4). From Fig. 2(d), it is seen that failure first occurs in compression when condition number 5 [Eqs. (3e)] is violated. As clearly manifested, the studied crystals do not show any instability

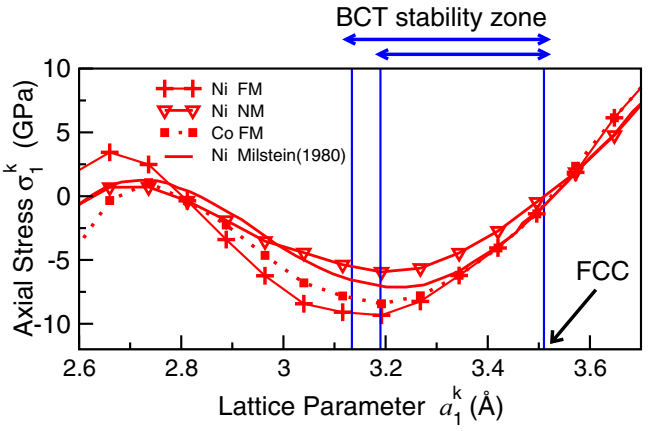


FIG. 4. Applied stress $\sigma_1^k$ along the tetragonal deformation path as a function of the compressed [001] axial parameter $a_1^k$. The blue vertical lines mark the values of the lattice parameters $a_1^k$ at which the lattice is stress-free (right line) or becomes unstable (left lines).

until reaching their inflexion points in compression. Contrary to the scenario taking place in tension [24] where Ni crystal bifurcates to orthorhombic phase ($C_{22} = C_{23}$) well below its inflexion point without increasing its elastic energy, here the crystals fail in compression because they can't support an additional compressive load.

Let us note that a similar research regarding the epitaxial deformation of nickel and cobalt in the (001) plane has already been performed by Zeleny *et al.* [40]. As can be seen from their Figs. 5(a) and 5(c), the total energies have a similar shape at biaxial deformation as the total energies in our Figs. 2(a) and 3(a). Also, the epitaxial stresses calculated in that paper [Figs. 5(b) and 5(d)] are similar in shape with uniaxial stresses exhibited in our Fig. 4.

## IV. Ni-RICH ALLOYS

In this section we present and discuss the main results of this study, i.e., MTCS of Ni-rich alloys. To begin with, we present in what follows the equilibrium lattice parameters ($a_{eq}$) of the stress-free Ni-6.25 at. % $X$ alloys and compare them with available experimental data. Both $a_{eq}$ and MTCS properties display clear trends with the number of $d$ electrons in the TM alloying elements.

### A. Lattice parameters

Before proceeding to the theoretical strength part, we examine here the lattice parameter expansion of the Ni

TABLE I. A comparison between our and other predicted values of the maximum theoretical compressive strengths (GPa)/strains (unitless) upon different uniaxial loading.

| Element | Phase | Method | ⟨001⟩ | ⟨110⟩ | ⟨111⟩ |
|---|---|---|---|---|---|
| Ni | fcc-FM | our work | 9.37/ − 0.08 | | |
| Ni | fcc-FM | PAW-VASP [26] | 9.4/ − 0.10 | N/A | 49.9/ − 0.15 |
| Ni | fcc-NM | our work | 5.93/ − 0.08 | | |
| Ni | fcc-NM | semiempirical [24] | 7.1/ − 0.091 | N/A | N/A |
| Co | fcc-FM | our work | 8.20/ − 0.1 | | |

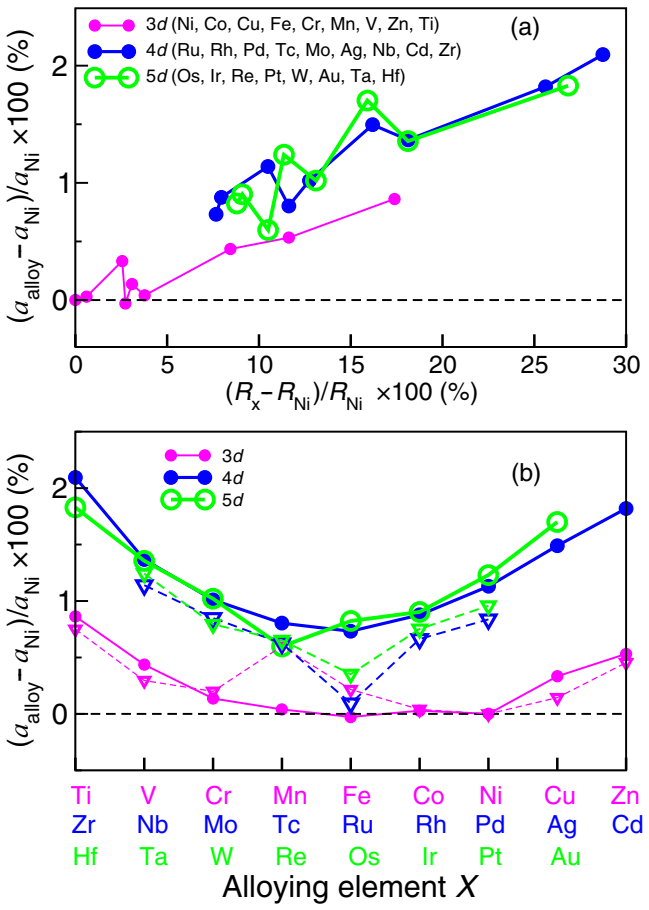


FIG. 5. (a) Equilibrium lattice expansion expressed in percent (%) as a function of (a) atomic-radius [41] difference (%) and (b) 3*d*, 4*d*, or 5*d* alloying element for alloy composition Ni-6.25 at. % *X*. The triangles mark data interpolated from experiments [42–48].

host-matrix upon alloying with 3*d*, 4*d*, and 5*d* TM elements. We recall that the calculations have been done on 128-atom supercells, including 8 alloying atoms. The supercells volume was relaxed and the atomic positions were locally minimized with respect to energy.

The lattice parameter for a known crystal structure, empirically, is related to the atomic radius, so the dependence of an alloy lattice parameter on the alloying element composition is typically explained by the atomic radius of alloying atoms, though there are few exception to this rule. In Fig. 5(a) the lattice expansion of Ni-6.25 at. % *X* is plotted against the alloying element (*X*)-solvent (Ni) atomic radius difference where datasets are classified according to the periods in the periodic table. The atomic radius of the investigated alloying element *X* is Wigner-Seitz radius (WS) obtained from the room temperature (RT) experimental atomic volumes ($V_{exp}^{RT}=\frac{4}{3}\pi WS^3$) of the alloying element ground state structure [41]. It is visible that the lattice expansion increases as a function of the alloying element radius, though the dependence is not strictly linear.

Figure 5(b) plots our predictions, along with the assessed experimental results [42–48], of the lattice expansion as a function of alloying element *d*-band filling. The experimental data correspond to alloys prepared at high temperature, well

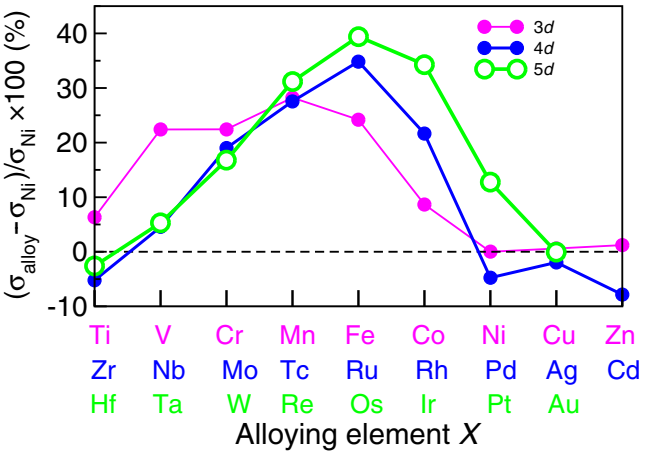


FIG. 6. Variation of the percent additional strength as a function of 3*d*, 4*d*, or 5*d* alloying element for alloy composition Ni-6.25 at. % *X*.

beyond 1000 K, high enough to be chemically disordered. Most of these alloys are most probably weakly ferromagnetic or paramagnetic at the temperatures where their lattice parameters have been measured. In accordance with the experimental data, all of the 4*d*, 5*d*, and most of 3*d* alloying elements induce an increase in the lattice expansion. Moreover, a nearly parabolic trend is observed for each of the 3*d*, 4*d*, and 5*d* series, with minima corresponding to the Fe/Ru/Os column. However, one notes a sudden increase in the lattice expansion for Mn and Fe alloying elements, contrary to the decreasing trend as a function of 3*d* electron count. This is due to the magnetism of Fe and Mn atoms in ferromagnetic Ni at room temperature [49,50].

It is important to note that, in spite of the large disparity in atomic radii existing within the 3*d* period, the magnitude of the resulting change in the lattice expansion parameter per 6.25 at. % alloying element addition is too small (0–0.8%), while alloying elements from 4*d* and 5*d* with comparable radii to the 3*d* alloying elements induce more important change (0.6–1.4%). However, all these alloying elements, except Hf and Zr, induce less than 1.35% change, and consequently they are compressed to a high degree in the fcc Ni lattice.

### B. Theoretical strength

Figure 6 plots the values of the MTCS for Ni-6.25 at. % *X* alloys as a function of the number of *d* electrons for the alloying elements (*X*). The strength displays a concave and an almost parabolic dependence on the alloying element *d* electron count for 4*d* and 5*d* series, with maximum values occurring at Ru and Os, respectively. For 3*d* series, we observe rather a plateau from V to Fe with a relatively small deviation for Mn. The general trend shown here is for the ideal strength to reach a maximum at approximately the Mn or Fe column of the periodic table. In particular, for the 5*d* elements, the maximum strength is predicted to occur at band filling slightly higher than Re. Additionally, we observe that the alloying elements of the column Fe/Ru/Os having the highest compressed values in the Ni matrix at ambient conditions [see Fig. 5(b)] produce the highest MTCS values.

Our findings show that alloying Ni with TM elements lying toward the center of the 3*d*, 4*d*, and 5*d* periods enhances considerably the strength of Ni-matrix, much more than alloying elements residing towards the peripheries, thanks to their well-known maximum cohesive energies [51–54]. In fact, it is well known that the bulk moduli of the 3*d*, 4*d*, and 5*d* TM elemental metals exhibit a parabolic trend, as shown by Pettifor [55] using canonical *d*-band theory and these trends have been confirmed by other authors, e.g., Rose and Shore [56]. Interestingly, de Jong *et al.* [57] observed, using small supercells, however, that alloying HCP-Re with elements of half *d*-band filling increases both bulk and shear moduli.

## V. CONCLUSIONS

The solid solution enhancement of the theoretical compressive strength associated with various TM elements alloyed with Ni was systematically investigated using DFT-based calculations. Since our calculations are quasistatic, they miss phonon-induced instabilities [12] near the inflexion point and may, therefore, overestimate the ideal strength.

We found fcc Ni and Co fail by compression and not by undergoing a phase transition. Additionally, we found the strength of FM Co to be larger than that of NM Ni by 27%, an observation of practical interest for Co-based materials. We predict a parabolic dependence of the strength of the alloys on the alloying element *d*-electrons number for 4*d* and 5*d* series, where alloying Ni with elements having half *d*-band filling gives rise to maximal strengthening, namely Os (40%), Ru (35%), Ir (34%), and Re (31%). Subsequently, the potency of the TM-alloying elements in improving the strength is clearly related to their *d*-electrons count. Our results are valid only for the compressive strength along the ⟨001⟩ loading direction, provided no phonon or other instability is encountered prior to reaching the inflexion point in the energy versus elongation curve, however we suggest that the observed strength peak associated with half *d*-band alloying elements is universal and hence is independent from strength-test type. A shearing of these alloys with respect to the most susceptible slip systems {111}⟨112⟩ is most probable to reproduce qualitatively similar parabolic trends with maxima situated at half *d*-band alloying elements.

## ACKNOWLEDGMENTS

A.B. and S.G.F. acknowledge funding by the Deutsche Forschungsgemeinschaft (DFG) through project C6 as the Collaborative Research Centre SFB/TR 103.

[1] F. Milstein, Phys. Rev. B **3**, 1130 (1971).
[2] A. Kelly and N. H. Macmillan, *Strong Solids* (Clarendon, Oxford, 1986).
[3] D. M. Clatterbuck, D. C. Chrzan, and J. W. Morris, Jr., Acta Mater. **51**, 2271 (2003).
[4] N. Nagasako, M. Jahnátek, R. Asahi, and J. Hafner, Phys. Rev. B **81**, 094108 (2010).
[5] T. Li, J. W. Morris, N. Nagasako, S. Kuramoto, and D. C. Chrzan, Phys. Rev. Lett. **98**, 105503 (2007).
[6] M. L. Jokl, V Vitek, and C. J. McMahon, Jr., Acta Metall. **28**, 1479 (1980).
[7] O. Rodríguez de la Fuente, J. A. Zimmerman, M. A. González, J. de la Figuera, J. C. Hamilton, W. W. Pai, and J. M. Rojo, Phys. Rev. Lett. **88**, 036101 (2002).
[8] Y. Ma, J. S. Tse, and D. D. Klug, Phys. Rev. B **67**, 140301 (2003).
[9] S. M.-M. Dubois, G.-M. Rignanese, T. Pardoen, and J.-C. Charlier, Phys. Rev. B **74**, 235203 (2006).
[10] P. Řehák, M. Černý, and J. Pokluda, J. Phys.: Condens. Matter **24**, 215403 (2012).
[11] O. M. Krasilnikov, M. P. Belov, A. V. Lugovskoy, I. Yu. Mosyagin, and Yu. Kh. Vekilov, Comput. Mater. Sci. **81**, 313 (2014).
[12] Recently, P. Řehák, M. Černý, and M. Šob, Modell. Simul. Mater. Sci. Eng. **23**, 055010 (2015) found that phonon and elastic instabilities of fcc Ni under uniaxial tension along ⟨100⟩ direction do occur at very close strains and showed that the predicted instabilities in Ni are of elastic nature.
[13] Edited by E. S. Huron, R. C. Reed, M. C. Hardy, M. J. Mills, R. E. Montero, P. D. Portella, and J. Telesman, *Superalloys 2012* (John Wiley & Sons, Inc., Hoboken, NJ, 2012).
[14] D. Roundy, C. R. Krenn, M. L. Cohen, and J. W. Morris, Phys. Rev. Lett. **82**, 2713 (1999).
[15] D. M. Clatterbuck, C. R. Krenn, M. L. Cohen, and J. W. Morris, Jr., Phys. Rev. Lett. **91**, 135501 (2003).
[16] M. Černý, P. Šesták, J. Pokluda, and M. Šob, Phys. Rev. B **87**, 014117 (2013).
[17] S. Chen, X. G. Gong, and S-H Wei, Phys. Rev. Lett. **98**, 015502 (2007).
[18] Y. Zhang, H. Sun, and C. Chen, Phys. Rev. Lett. **93**, 195504 (2004).
[19] X. Blase, P. Gillet, A. San Miguel, and P. Mélinon, Phys. Rev. Lett. **92**, 215505 (2004).
[20] C. Jiang and S. G. Srinivasan, Nature (London) **496**, 339 (2013).
[21] Y.-J. Wang and C.-Y. Wang, Appl. Phys. Lett. **94**, 261909 (2009).
[22] G. Grimvall, B. Magyari-Köpe, V. Ozoliņš, and K. A. Persson, Rev. Mod. Phys. **84**, 945 (2012).
[23] J. Pokluda, M. Černý, M. Šob, and Y. Umeno, Prog. Mater. Sci. **73**, 127 (2015).
[24] F. Milstein and B. Farber, Phys. Rev. Lett. **44**, 277 (1980).
[25] M. Černý and J. Pokluda, Phys. Rev. B **82**, 174106 (2010).
[26] M. Černý and J. Pokluda, Comput. Mater. Sci. **50**, 2257 (2011).
[27] Y.-L. Liu, Y. Zhang, H.-B. Zhou, G.-H. Lu, and M. Kohyama, J. Phys.: Condens. Matter **20**, 335216 (2008).
[28] R. Hill and F. Milstein, Phys. Rev. B **15**, 3087 (1977).
[29] J. M. Cowley, J. Appl. Phys. **21**, 24 (1950).
[30] B.E. Warren, *X-ray diffraction* (New York, Dover, 1990).
[31] P. E. Blöchl, Phys. Rev. B **50**, 17953 (1994).
[32] G. Kresse and J. Hafner, Phys. Rev. B **47**, 558 (1993).
[33] G. Kresse and J. Hafner, Phys. Rev. B **49**, 14251 (1994).
[34] G. Kresse and J. Furthmüller, Comput. Mater. Sci. **6**, 15 (1996).
[35] J. P. Perdew, K. Burke, and M. Ernzerhof, Phys. Rev. Lett. **77**, 3865 (1996).
[36] H.-J. Monkhorst and J.-D. Pack, Phys. Rev. B **13**, 5188 (1976).
[37] A. V. Ruban, S. Khmelevskyi, P. Mohn, and B. Johansson, Phys. Rev. B **75**, 054402 (2007).

[38] J. Giber, R. Drube, and V. Dose, Appl. Phys. A **52**, 167 (1991).
[39] N. W. Ashcroft and N. D. Mermin, *Solid State Physics* (Thomson Learning, Orlando, USA, 1976).
[40] M. Zelený, D. Legut, and M. Šob, Phys. Rev. B **78**, 224105 (2008).
[41] All WS Radii of the concerned alloying elements are determined from C. Kittel, *Introduction to Solid State Physics*, 7th ed. (Wiley, New York, 1996) except for Manganese radius, it is obtained from Ref. [58].
[42] Y. Mishima, S. Ochiai, and T. Suzuki, Acta Metall. **33**, 1161 (1985).
[43] A. Nash and P. Nash, Bull. Alloy Phase Diagrams **5**, 403 (1984).
[44] P. Nash, Bull. Alloy Phase Diagrams **6**, 124 (1985).
[45] B. Predel, Ni-Ru (Nickel-Ruthenium), *Ni-Np–Pt-Zr* (Springer, Berlin, Heidelberg, 1998), pp. 1–3.
[46] A S Pavlovic, V Suresh Babu, and Mohindar S Seehra, J. Phys.: Condens. Matter **8**, 3139 (1996).
[47] E. Bucher, W. F. Brinkman, J. P. Maita, and A. S. Cooper, Phys. Rev. B **1**, 274 (1970).
[48] T. Ya. Velikanova, T. G. Mazhuga, O. L. Semenova, P. S. Martsenyuk, and V. M. Vereshchaka, Powder Metallurgy and Metal Ceramics **41**, 288 (2002).
[49] H. Tange, T. Tokunaga, and M. Goto, J. Phys. Soc. Jpn. **45**, 105 (1978).
[50] H. E. H. Stremme, Phys. Lett. A **46**, 126 (1973).
[51] M. Cyrot and F. Cyrot-Lackmann, J. Phys. F **6**, 2257 (1976).
[52] F. Cyrot-Lackmann, J. Phys. Chem. Solids **29**, 1235 (1968).
[53] J. Friedel, in *Physics of Metals*, edited by J. M. Ziman (Cambridge University Press, New York, 1969).
[54] D. G. Pettifor, Solid State Phys. **40**, 43 (1987).
[55] D. G. Pettifor and R. Podloucky, J. Phys. C **19**, 315 (1986).
[56] J. H. Rose and H. B. Shore, Phys. Rev. B **49**, 11588 (1994).
[57] M. de Jong, D. L. Olmsted, A. van de Walle, and M. Asta, Phys. Rev. B **86**, 224101 (2012).
[58] J. A. C. Marples, Phys. Lett. A **24**, 207 (1967).